

Compartment-Specific Regulation of Plasma Membrane Calcium ATPase Type 2 in the Chick Auditory Brainstem

YUAN WANG, DALE E. CUNNINGHAM, BRUCE L TEMPEL, AND EDWIN W RUBEL*

Virginia Merrill Bloedel Hearing Research Center, Department of Otolaryngology-Head and Neck Surgery, University of Washington School of Medicine, Seattle, Washington 98195

ABSTRACT

Calcium signaling plays a role in synaptic regulation of dendritic structure, usually on the time scale of hours or days. Here we use immunocytochemistry to examine changes in expression of plasma membrane calcium ATPase type 2 (PMCA2), a high-affinity calcium efflux protein, in the chick nucleus laminaris (NL) following manipulations of synaptic inputs. Dendrites of NL neurons segregate into dorsal and ventral domains, receiving excitatory input from the ipsilateral and contralateral ears, respectively, via nucleus magnocellularis (NM). Deprivation of the contralateral projection from NM to NL leads to rapid retraction of ventral, but not the dorsal, dendrites of NL neurons. Immunocytochemistry revealed symmetric distribution of PMCA2 in two neuropil regions of normally innervated NL. Electron microscopy confirmed that PMCA2 localizes in both NM terminals and

NL dendrites. As early as 30 minutes after transection of the contralateral projection from NM to NL or unilateral cochlea removal, significant decreases in PMCA2 immunoreactivity were seen in the deprived neuropil of NL compared with the other neuropil that continued to receive normal input. The rapid decrease correlated with reductions in the immunoreactivity for microtubule-associated protein 2, which affects cytoskeleton stabilization. These results suggest that PMCA2 is regulated independently in ventral and dorsal NL dendrites and/or their inputs from NM in a way that is correlated with presynaptic activity. This provides a potential mechanism by which deprivation can change calcium transport that, in turn, may be important for rapid, compartment-specific dendritic remodeling. *J. Comp. Neurol.* 514: 624–640, 2009. © 2009 Wiley-Liss, Inc.

Indexing terms: calcium homeostasis; afferent regulation; dendritic remodeling; activity dependence; nucleus laminaris

The development and maintenance of neuronal dendritic structure are greatly influenced by synaptic input. In a variety of neuronal systems, manipulations of excitatory inputs lead to changes in the overall orientation of dendritic trees (Harris and Woolsey, 1981), the specific pattern of dendritic branching (Deitch and Rubel, 1984; Cline, 2001; Wong and Ghosh, 2002; Sorensen and Rubel, 2006), as well as the density and distribution of dendritic spines (Yuste and Bonhoeffer, 2001, 2004; Van Aelst and Cline, 2004). Although the cellular processes underlying this influence are still relatively unknown, elevations in intracellular calcium concentration ($[Ca^{2+}]_i$) resulting from manipulations of synaptic inputs have been associated with changes in dendritic morphology (Chen and Ghosh, 2005; Lohmann and Wong, 2005; Redmond and Ghosh, 2005). Potential roles of calcium influx, either via neurotransmitter-mediated receptors and voltage-gated calcium channels or via release of calcium from intracellular organelles, have been investigated following manipulations of synaptic inputs (Hille, 1994; Lohmann et al., 2002; Nimchinsky et al., 2002; Chen et al., 2005). However, little is known about how the various systems that normally regulate $[Ca^{2+}]_i$, particularly calcium efflux pathways, contribute to dendritic changes in response to changes in synaptic inputs.

One useful experimental model for studying afferent regulation of dendritic structure is the third-order auditory neurons of the nucleus laminaris (NL) in the avian brainstem (Benes et al., 1977; Deitch and Rubel, 1984; Sorensen and Rubel, 2006; Wang and Rubel, 2008). NL appears to function as a coincidence detector system for binaural hearing (Young and Rubel, 1983, 1986; Carr and Konishi, 1988, 1990; Overholt et al., 1992; Joseph and Hyson, 1993) and is thought to function analogously to the medial superior olivary nucleus of mammals (Burger and Rubel, 2008). Dendrites of each NL neuron segregate into dorsal and ventral domains, receiving excitatory

Grant sponsor: National Institute on Deafness and Other Communication Disorders; Grant number: DC-03829; Grant number: DC-02739; Grant number: DC-04661; Grant number: DC-00018.

*Correspondence to: Edwin W Rubel, Virginia Merrill Bloedel Hearing Research Center, Mail Stop 357923, University of Washington, Seattle, WA 98195. E-mail: rubel@u.washington.edu

Received 31 December 2008; Revised 18 February 2009; Accepted 24 February 2009

DOI 10.1002/cne.22045

Published online March 18, 2009 in Wiley InterScience (www.interscience.wiley.com).

input almost exclusively from the ipsilateral and contralateral ears, respectively, via the nucleus magnocellularis (NM) on each side of the brain (Parks and Rubel, 1975). Consequently, excitatory inputs to one set of NL dendrites can be altered by manipulating the ipsilateral or contralateral projection of NM neurons, while leaving the input to the other dendritic domain structurally and functionally intact (Born et al., 1991). Previous studies in chicks have demonstrated rapid retraction of the ventral NL dendrites within hours after transection of the contralateral NM projection, whereas the dorsal NL dendrites, receiving intact input, appear largely unaffected (Benes et al., 1977; Deitch and Rubel, 1984, 1989; Sorensen and Rubel, 2006). These studies demonstrated the NL as a suitable model with unique benefits in studying local dendritic reorganization with a matched intracellular control. However, in contrast to systematic studies on the structural changes of NL dendrites following manipulations of synaptic input, molecular mechanisms underlying these changes have not been investigated.

NL neurons in chicks exhibit high spontaneous and acoustic-driven discharge rates (Born et al., 1991), suggesting that NL neurons require a highly efficient calcium-regulatory system to maintain normal $[Ca^{2+}]_i$. Multiple calcium efflux systems may coexist within NL dendrites, including the intracellular organelle storage system, the Na^+/Ca^{2+} exchanger, the plasma membrane calcium ATPase (PMCA), and calcium binding proteins. Among these, the PMCA family is a group of transmembrane proteins expelling calcium out of the cell. PMCA has a high affinity for calcium and is a major calcium efflux system that sets the resting calcium concentration (Carafoli, 1987; Thayer et al., 2002; Duman et al., 2008). Among four types of PMCA, PMCA2 is the most active pump (Elwess et al., 1997; Brini et al., 2003). Mutations in the PMCA2 gene lead to hearing loss and vestibulomotor deficits in mice (Street et al., 1998; McCullough and Tempel, 2004; Tempel and Shilling, 2007). With the use of immunocytochemistry, the present study demonstrates remarkably dense expression of PMCA2 in NL neuropil regions and rapid decreases in PMCA2 immunoreactivity following afferent deprivation. The current paper, along with our recent study on microtubule-associated protein 2 (MAP2) in NL dendrites (Wang and Rubel, 2008), is our first effort to explore the molecular substrates underlying dendritic regulation in NL neurons.

MATERIALS AND METHODS

White leghorn chick hatchlings (*Gallus domesticus*) 4–11 days of age were used. In addition, 6-week-old CBA/CaJ deafwaddler (*dfw^{2J}*) mice (Street et al., 1998) and their wild-type littermates were used for comparison in Western blot analysis. All procedures were approved by the University of Washington Institutional Animal Care and Use Committee and conformed to NIH guidelines. All efforts were made to minimize pain or discomfort of the animals and to minimize the number of the animals used.

Transection of the crossed dorsal cochlear tract (XDCT)

Animals were anesthetized with a mixture of 40 mg/kg ketamine and 12 mg/kg xylazine. The animals were placed in a head holder, and surgery was conducted by using the method of Deitch and Rubel (1984). Briefly, the neck muscles were resected to expose the dura covering the cerebellomedullary

cistern. An ophthalmic knife was inserted through the dura and the fourth ventricle and into the brainstem to transect the XDCT at the midline. The wound was packed with gelfoam and sealed with a tissue adhesive, LiquiVet (Oasis Medical, Mettawa, IL). The location and extent of the transection were examined after further tissue processing (see below). In total, 23 animals received a complete transection of XDCT. Four were allowed to survive for 0 hours, six for 0.5 hours, five for 3 hours, three for 6 hours, and five for 14 hours. The 0-hour survival time refers to an immediate perfusion (less than 5 minutes) after the surgery. These cases served as a second set of controls, in addition to unoperated animals ($n = 6$). In addition, five animals received midline incisions that were either caudal or rostral to the XDCT, without damaging NM neurons or their axons, and survived for 0.5–12 hours. These cases served as sham-operated controls.

Cochlea removal

The procedure described by Born and Rubel (1985) was used. Animals were anesthetized as described above. A small incision was made to widen the external auditory meatus of the ear, and the tympanic membrane and columella were removed to expose the oval window. The basilar papilla, including the lagena macula, was removed via the oval window using fine forceps, floated on water, and examined with a surgical microscope to verify complete removal. Only animals with a complete removal of the basilar papilla, including the lagena, were used for further tissue processing and data analysis. The cochlear duct was packed with a small piece of gelfoam. The incision was sealed with LiquiVet adhesive. This procedure results in complete removal of the basilar papilla but spares the ganglion cells, which subsequently die over the next few weeks (Born and Rubel, 1985). In total, 38 animals received a unilateral cochlea removal (right ear). Four were allowed to survive for 0 hours, four for 0.5 hours, 12 for 3 hours, nine for 6 hours, and nine for 14 hours. In addition, five animals received bilateral cochlea removal and survived for 3 hours.

Immunocytochemistry

The animals were anesthetized and transcardially perfused with 0.9% saline, followed by 4% paraformaldehyde in 0.1 M phosphate buffer. The brains were removed from the skull and postfixed overnight in the same fixative. Completeness of the XDCT transection was verified under a microscope after removal of the cerebellum, and incomplete cases were discarded. The brains were then either transferred to 30% sucrose in phosphate-buffered saline (PBS; pH 7.4) until they sank and cut coronally at 30 μ m on a freezing sliding microtome or washed in PBS and cut coronally at 40 μ m on a vibratome. Sections were collected in PBS into four alternate series, each containing eight or nine sections through NL. Alternate sets of one in four sections were stained for Nissl substance or immunocytochemically for PMCA2, SNAP-25, and MAP2 by peroxidase or fluorescent immunocytochemical methods. Briefly, free-floating sections were incubated with primary antibody solutions diluted 1:1,000 in PBS with 0.3% Triton X-100 overnight at 4°C, followed by biotinylated anti-IgG antibodies (1:200; Vector Laboratories, Burlingame, CA) or AlexaFluor secondary antibodies (1:200; Molecular Probes, Eugene, OR) for 2 hours at room temperature.

For peroxidase immunocytochemical staining, sections were incubated in avidin-biotin-peroxidase complex solution (ABC Elite kit; Vector Laboratories) diluted 1:100 in PBS with 0.3% Triton X-100 for 1 hour at room temperature. Sections were incubated for 3–7 minutes in 0.015% 3,3'-diaminobenzidine (Sigma, St. Louis, MO), either with 0.01% hydrogen peroxide in PBS or with 0.03% hydrogen peroxide, 125 mM sodium acetate, 10 mM imidazole, and 100 mM nickel ammonium sulfate. Sections were mounted on gelatin-coated slides and then dehydrated, cleared, and coverslipped with DPX mounting medium (EMS, Hatfield, PA). For fluorescent immunocytochemical staining, sections were mounted and coverslipped with Fluoromount-G (Southern Biotechnology, Birmingham, AL).

Primary antibodies

Polyclonal anti-PMCA2 (catalog No. PA1-915) made in rabbit was purchased from Affinity Bioreagents (Golden, CO). The immunogen is a synthetic peptide corresponding to amino acid residues 5–19 of human PMCA2 protein. The sequence of the immunogen is TNSDFYSKNQRNESS. This sequence is completely conserved between human and rat PMCA2. According to the data sheet provided by the manufacturer, this antibody detects an ~127-kDa protein and an ~133-kDa protein in Western blot analysis that corresponds to PMCA2a and PMCA2b, respectively, from rat brain microsomal fractions. The corresponding sequence in the chick PMCA2, TNSDFYSKNQRNEAN, varies from the human sequence only at the last two amino acids. The specificity of the antibody for detecting the chick PMCA2 was tested by Western blot analysis in the cerebellum (Sepúlveda et al., 2007) and in the dorso-caudal brainstem in the current study (see below).

Monoclonal anti-SNAP-25 (catalog No. MAB331) made in mouse was purchased from Chemicon International (Temecula, CA). The immunogen is human crude synaptic immunoprecipitate. The antibody recognizes a band of 26–27 kDa in Western blot analysis. Monoclonal anti-MAP2 (catalog No. MAB3418) made in mouse was purchased from Chemicon International. The immunogen is bovine brain microtubule protein. The antibody binds specifically to MAP2a and MAP2b and is detected as a 300-kDa band in Western blot analysis. This antibody has been used in the chick auditory brainstem in a previous study from our laboratory (Wang and Rubel, 2008).

Western blotting

Western blot immunoassay was conducted to confirm that the anti-PMCA2 antibody used in the present study recognizes similar proteins in chicks compared with mammals. Protein samples were harvested from the NL/NM and the surrounding region in the dorsocaudal brainstem of chicks and the whole brain of mice. An additional whole-brain sample from the *dfw^{2J}* homozygous mutant mouse that is known to lack PMCA2 immunoreactivity (McCullough and Tempel, 2004) was used as a negative control. All samples were homogenized in lysis buffer (20 mM NaF, 1 mM Na vanadate, 0.5% Triton X-100, 0.1% SDS, 10 mM Tris, and 150 mM NaCl) with protease inhibitor cocktail (catalog No. P8340; Sigma). Protein concentrations were determined by using BCA Protein Assay (Pierce, Rockford, IL). Each sample (5 μ g or 12.5 μ g protein) was boiled for 5 minutes to denature protein and loaded onto a 4–20% SDS-polyacrylamide gel (Bio-Rad, Hercules, CA). The gel was run for 100 minutes at 100 V. Protein

was then electroblotted to a PVDF membrane (Bio-Rad). Membranes were blocked in 5% nonfat milk in TBS (10 mM Tris and 150 mM NaCl) and probed with the PMCA2 antibody (1:1,000). Horseradish peroxidase (HRP)-conjugated secondary antibodies (1:3,000; Bio-Rad) were used for detection with enhanced chemiluminescent reagents (ECL; Amersham, Little Chalfont, Buckinghamshire, England). An antibody against β -actin (Abcam Inc, Cambridge, MA) was used as a protein loading control.

Transmission electron microscopy

Two chicks were anesthetized and transcardially perfused with 0.9% saline followed by 2% paraformaldehyde and 0.05% glutaraldehyde in 0.1 M acetate buffer (pH 6.0) for 5 minutes and then by the same concentration of aldehydes in 0.06 M borate buffer (pH 8.5) for 20 minutes (Berod et al., 1981; Bodor et al., 2005). Brains were dissected and then immersed in the latter fixative for 40 minutes. Brains were washed in 0.1 M phosphate buffer (PB), and coronal sections of the brainstem containing NM and NL were cut on a vibratome at 50 μ m. Sections were cryoprotected in 10%, 20%, and 30% sucrose in PB prior to three freeze-thaw cycles in liquid nitrogen. Sections were treated with 0.5% sodium borohydride for 15 minutes and returned to 0.1 M PB.

Blocking was performed in a solution containing 5% normal goat serum, 0.8% BSA, 0.1% cold water fish skin gelatin, 0.05% sodium azide in 50 mM Tris buffer (pH 7.4) for 1 hour. This solution was replaced with a 1:1,000 dilution of rabbit anti-PMCA2 in the same buffer overnight at 4°C with gentle agitation. Several sections were maintained in the blocking buffer as a no-primary control. After washes, sections were incubated in a 1:50 dilution of goat anti-rabbit ultrasmall (0.6 nm) gold (No. 25101; EMS) for 2 hours. Additional washes were performed prior to incubation in a 1:10 dilution of Enhancement Conditioning Solution (No. 25830; EMS) and subsequent silver enhancement. After washes, the sections were treated with 1% OsO₄ for 2 minutes, followed by 0.5% OsO₄ for 20 minutes, both in 0.1 M PB. Sections were washed, dehydrated, and embedded in Eponate 12 resin (Ted Pella, Inc., Redding, CA) prior to obtaining ultrathin sections. After remounting of the vibratome sections on blank resin stubs, 100-nm ultrathin sections were made from the surface (1–2 μ m) of the immunoreacted sections. Ultrathin sections were mounted on 200-mesh, Athene thin bar grids (Ted Pella, Inc.), contrasted with uranyl acetate and lead citrate, and viewed in a JEOL 1200 EX transmission electron microscope.

Data analysis in NL

Both XDCT transection and unilateral cochlea removal compromise the excitatory activity to one dendritic domain of NL (referred to here as the *deprived domain*) and leave the afferent activity to another domain uncompromised (referred to here as the *intact domain*). The structure and function of the intact domain of NL are largely unchanged following the manipulations used here (Lippe et al., 1980; Deitch and Rubel, 1984, 1989; Born et al., 1991), so the change in the density of PMCA2 immunoreactivity in the deprived domain was estimated by the difference between two neuropil domains. This method was adopted to avoid potential inconsistencies caused by variations in immunostaining between cases (Lippe et al., 1980; Durham and Rubel, 1985; Born et al., 1991; Wang and Rubel, 2008). In our preparations, the staining intensity of

PMCA2 in the intact domain of NL neuropil was qualitatively similar before and after the manipulations (see Figs. 6, 9). Thus, we assume that the differences of PMCA2 immunoreactivity between two neuropil domains were due largely to the changes in the deprived neuropil. However, the methods used in the current study could not determine the subcellular compartment(s) in which PMCA2 changes occurred in response to our manipulations. In addition, PMCA2 immunoreactivity within the cell body layer, which contains NL neuronal somata and laterally oriented, short dendritic branches (Smith, 1981), was excluded from the analyses described below.

Two types of analyses were conducted to quantify relative differences between the dorsal and the ventral neuropil domains of NL with respect to PMCA2 immunoreactivity within the first 14 hours following the manipulations. First we measured and compared the average density of the immunostaining between the deprived and the intact domains in the same region of NL. At least three cases were chosen for this analysis from each survival time and manipulation group. For each case, sections 2, 4, and 6, (counting from caudal to rostral) from those sets of sections stained with peroxidase were chosen as representative of the caudal, intermediate, and rostral portion of NL, respectively. The levels of these sections are comparable to those illustrated in Figure 1 of Wang and Rubel (2008). For each section, three or four photomicrographs were taken of NL with a $\times 63$ oil-immersion objective (NA 1.40) at a total magnification of $\times 756$. The boundaries of the NL neuropil were evident in PMCA2 staining and were further verified by adjacent sections stained for Nissl. Average optical density of the dorsal and ventral NL neuropil domains was measured in Image J software (version 1.38X; National Institutes of Health). In all cases, the comparison of the average density between the dorsal and the ventral neuropil domains was made within the same photomicrograph from the same tissue section to avoid any possible inconsistencies caused by variations in immunostaining between cases and sections and variations in brightness across photomicrographs. We defined D and V as the average density of staining in the dorsal and ventral neuropil domains, respectively. The percentage difference (PD) was calculated as the change in the density of deprived neuropil domain relative to the intact domain, which is $(V - D)/D \times 100$ for both sides following XDCT transection and the contralateral side following unilateral cochlea removal and $(D - V)/V \times 100$ for the ipsilateral side following unilateral cochlea removal. The PDs from a single animal (or in the case of unilateral cochlea removal from each side of the brain) were averaged, and this mean PD represented a single data point for statistical analyses. These mean PDs from all animals of the same group were averaged and plotted as a function of survival time. Error bars are conservatively based on all of the data from each animal.

Correlation between changes in PMCA2 and dendritic structure following deprivation was estimated by plotting the PDs of PMCA2 immunoreactivity against the PDs of MAP2 immunoreactivity from nine animals that received unilateral cochlea removal. Average density of the immunoreactivities was measured as described above from sections double labeled for both PMCA2 and MAP2 with fluorescent immunocytochemical staining. These sections were chosen from the caudal portion of the nucleus at the level comparable to Figure 1A of Wang and Rubel (2008), because significant changes

in MAP2 immunoreactivity were detected in the caudal NL (Wang and Rubel, 2008). Two channels were imaged sequentially with an Olympus FV-1000 confocal microscope to avoid bleed-through between channels.

A second type of analysis was conducted to evaluate the overall change in the density of PMCA2 staining as a function of dendritic position (proximal vs. distal) from the NL neuron soma. Representative sections with a PD value smaller than -20 were chosen for this analysis from the cases that survived 0.5–6 hours following XDCT transection. Each neuropil domain was divided into subzones from proximal (adjacent to the soma) to distal dendrites at intervals of $5 \mu\text{m}$. The PD between the deprived and the control domains was calculated between comparable subzones at the same distance from the same NL neuron somata.

Significance was determined by using one-way ANOVA followed by Tukey's multiple-comparisons test or two-way ANOVA followed by Bonferroni posttest, in the Prism v. 5 software package (GraphPad Software, Inc., San Diego, CA). $P < 0.05$ was considered statistically significant. All data are shown as mean ± 1 SD in the text and figures.

Data analysis in NM

In the group that received unilateral cochlea removal, changes in the density of PMCA2 immunostaining were quantified between the ipsilateral and the contralateral NM from individual tissue sections. For each case, three images were taken from each side of NM with a $\times 20$ air objective (NA 0.75) at a total magnification of $\times 240$. Average optical density was measured within a square placed in the middle of the nucleus. The diameter of the square is $100 \mu\text{m}$ when measuring from the sections through the caudal and intermediate NM and $60 \mu\text{m}$ when measuring from the sections through the rostral NM. The PD was calculated as the change in staining density of the ipsilateral deprived NM relative to the contralateral intact NM. The PDs from all three samples from the same animal were averaged, and then these means from all animals of the same group were averaged and plotted as a function of survival time.

Digital imaging. Digital images of selected sections with peroxidase staining were captured with a Zeiss AxioPlan 2ie equipped with a CoolSnap HQ monochrome digital camera (Princeton Instruments, Trenton, NJ) and collected in Slidebook (version 4.0.2.8; Intelligent Imaging Innovations, Denver, CO). Fluorescent images were collected on a Fluoview-1000 laser scanning confocal microscope equipped with an IX-81 inverted microscope (Olympus America, Center Valley, PA). Image contrast and brightness adjustments and photomontages were made in Adobe Photoshop (Adobe Systems Inc., Mountain View, CA).

RESULTS

Western blotting

Western blot immunoassay was conducted to confirm that the anti-PMCA2 antibody used in the current study recognizes similar proteins in chickens compared with mammals. The results shown in Figure 1 illustrate nearly identical band (~ 130 kDa) recognition between chick and wild-type mouse. This band corresponds to the PMCA2 previously identified in the mouse (McCullough and Tempel, 2004). This band was absent

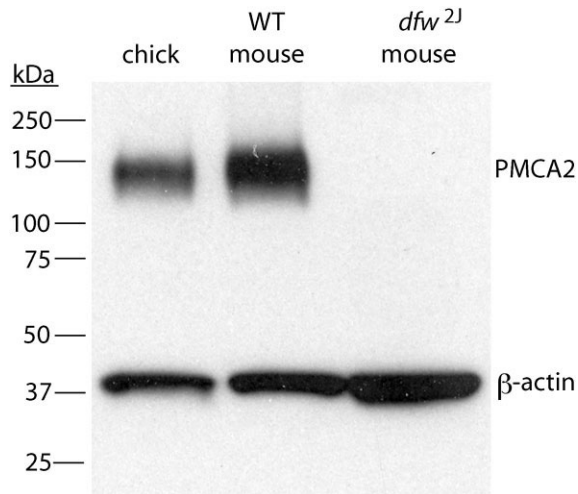


Figure 1. Western blot assay of anti-PMCA2 in tissues from chicks, wild-type (WT) mice, and *dfw^{2J}* mice. Molecular weight standards (left) were used to determine relative sizes of labeled protein. Lanes 1 and 2 were loaded with approximate 5 μ g of total protein. Chicken reactivity is nearly identical to that in the wild-type mouse with respect to the molecular weights at \sim 130 kDa. The *dfw^{2J}* lane was loaded with 12.5 μ g of total protein and showed no evidence of PMCA2 protein of the correct molecular weight.

in the *dfw^{2J}* mutant mice, which are known to lack PMCA2 immunoreactivity and have hearing and balance deficits.

Distribution and localization of PMCA2 in the normal NL and NM

In chicks, NL neurons are arranged in a single layer, except in the most caudolateral region of the nucleus, where multiple layers of neurons are present. Dendrites of NL neurons are segregated into dorsal and ventral domains that are bordered by two glial-rich layers. Immunocytochemistry revealed that PMCA2 is expressed at high levels throughout the NL neuropil region and around cell bodies, where NM terminals form synapses with NL neurons. Symmetric distribution of PMCA2 in the dorsal and ventral neuropil of NL formed two dense bands separated by a lightly stained cell body layer where the immunoreactivity was found mostly around the somata (Fig. 2A,B,D,G). The major immunoreactivity in the neuropil region overlapped with the immunoreactivity for MAP2, a neuronal somatodendritic marker (Fig. 2D–F), and was confined between the two glial layers (Fig. 2G–I). The average densities of PMCA2 immunoreactivity in the ventral and dorsal neuropil regions were not qualitatively different, and quantitative measurements did not reveal any statistically significant differences. Within NM, most neurons are adendritic or have only a single, short primary dendrite in P4–P10 chicks (Conlee and Parks, 1983). Immunoreactivity for PMCA2 was located perisomatically in NM neurons (Fig. 2C). In addition, immunoreactivity was also observed surrounding a number of smaller nuclei in NL neuropil regions and the adjacent glial layers (inset of Fig. 2B) as well as in NM (Fig. 2C). These nuclei are 5–8 μ m in diameter, suggesting that PMCA2 immunoreactivity is present on some glial cells. This suggestion is supported by the presence of PMCA2 in the mammalian astrocytes

(Fresu et al., 1999; Blaustein et al., 2002). Regions surrounding NL and NM are rich in axons and glial processes and did not contain distinct PMCA2 immunoreactivity.

Double labeling of PMCA2 and a presynaptic marker SNAP-25 demonstrated a certain degree of colocalization of the two antigens within NM and NL (white arrows, Fig. 3). However, cellular structures labeled with PMCA2 but lacking SNAP-25 were also widely detected (white arrowheads, Fig. 3). TEM observation confirmed that PMCA2 is localized in both pre- and postsynaptic compartments in the neuropil region of NL (Fig. 4), consistent with observations in mammals (Stauffer et al., 1997; DeMarco and Strehler, 2001; Burette and Weinberg, 2007; Jensen et al., 2007; Burette et al., 2009).

PMCA2 immunoreactivity in NL following XDCT transection

The XDCT contains the decussating NM axons that project to the ventral NL on both sides of the brain. A complete transection of XDCT at the midline eliminates the excitatory input to the ventral dendrites of NL neurons, while leaving the input to the dorsal dendrites intact (Fig. 5A,C). After XDCT transection, the afferent terminals from NM on the ventral NL dendrites do not show significant atrophic changes at the electron microscopic level during the first 4 hours (Deitch and Rubel, 1989).

The relative change in PMCA2 immunoreactivity in the deprived ventral neuropil compared with the intact dorsal neuropil exhibited a time-dependent pattern (Figs. 6, 7). Immediately after the surgery (0 hours), no reliable difference in the density of staining was observed between the two neuropil domains (Fig. 6B), and quantitative analyses supported this observation. The percentage difference (PD) of the staining density in the ventral neuropil compared with the dorsal neuropil (0.0 ± 8.5) was not significantly different from that of the unoperated control (-2.8 ± 1.3 ; Fig. 7A). Thirty minutes later, however, the ventral neuropil exhibited notably lower density of PMCA2 immunoreactivity compared with the dorsal neuropil in all but one case (Fig. 6C). The average PD across all six cases was -25.6 ± 23.9 . At 3–14 hours following the transection, a relatively lower density of staining in the ventral neuropil was detected consistently with the average PD of -32.0 ± 3.9 at 3 hours, -26.9 ± 5.2 at 6 hours, and -23.7 ± 8.0 at 14 hours (Figs. 6D–F, 7A). These PD values were significantly smaller than the unoperated controls at all four survival periods ($P_s < 0.001$).

Changes in the density of PMCA2 immunoreactivity in the ventral neuropil occurred symmetrically on both sides of the brain (Fig. 5C). On each side, the change was detected throughout the rostrocaudal and lateromedial extent of the nucleus (Fig. 7B). A two-way ANOVA (survival time by position) did not yield significant interaction between these two parameters, indicating the overall effect of the manipulation on the staining density does not vary with the position of the dendrites along the rostrocaudal axis of the nucleus. A slightly smaller mean of PD in the caudal NL than in the intermediate and rostral NL may be due to differential neuronal arrangements between the caudal and the other regions of NL. At any given location of the NL, the difference in the density of PMCA2 staining between the two neuropil domains was distributed throughout its proximal and distal extent (Fig. 8). Each subzone of the ventral neuropil exhibited a dramatic decrease of staining in comparison with the analogous subzone in the

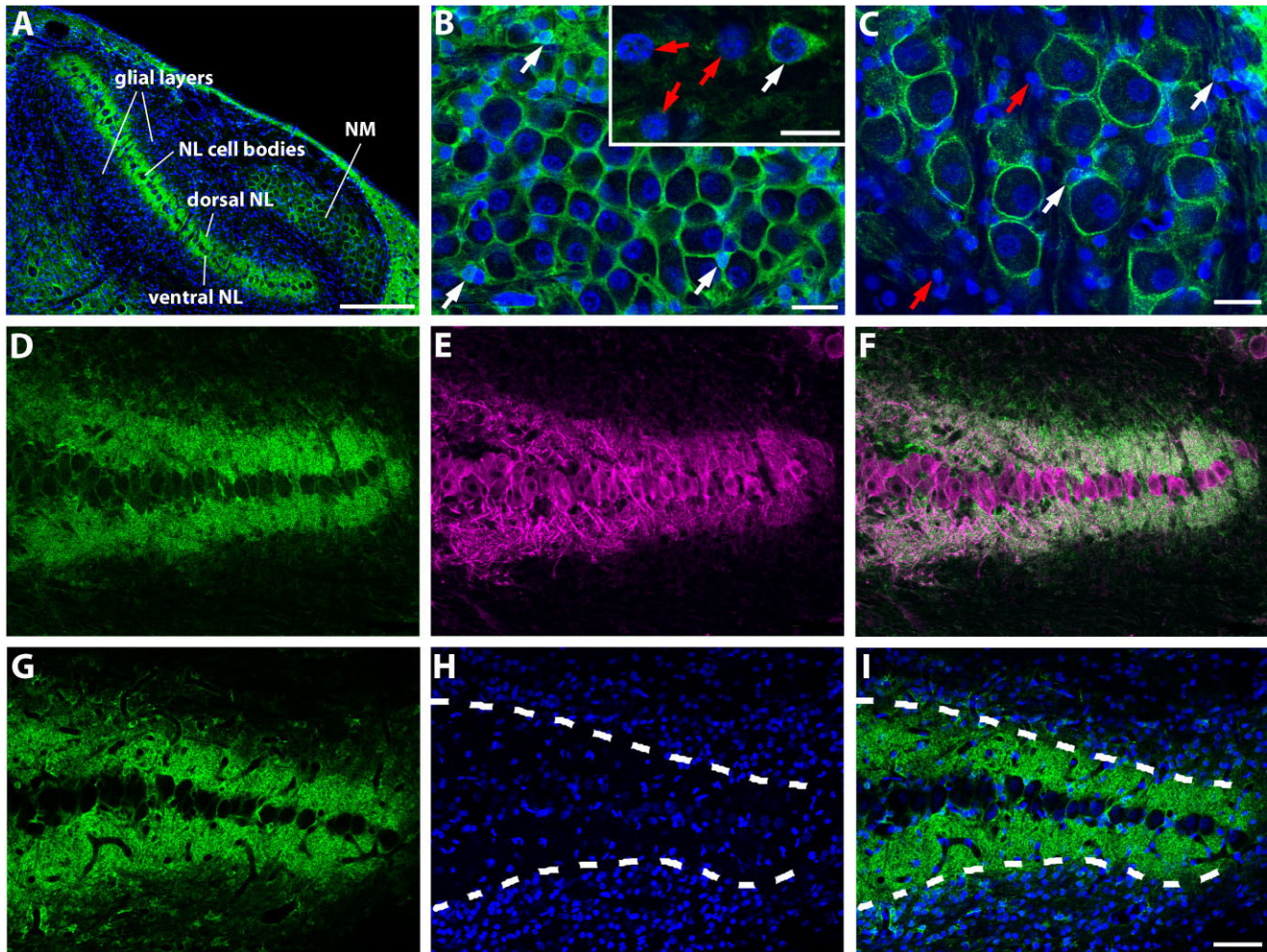


Figure 2. PMCA2 immunoreactivity in the NL and NM under control conditions. **A:** A low-magnification photomicrograph showing the overall pattern of PMCA2 immunoreactivity in NM and NL. **B,C:** High-magnification photomicrographs showing the perisomatic staining of PMCA2 in the caudal NL (**B**) and NM (**C**). Sections were doubly labeled with PMCA2 (green) and a nuclear marker DAPI (blue). Red and white arrows indicate unstained and stained glial cells, respectively. The inset in **B** was taken from the ventral glial layer of NL. **D–F:** Double labeling of PMCA2 (green) and a somatodendritic marker MAP2 (magenta) in NL. Merged image in **F**. **G–I:** Double labeling of PMCA2 (green) and DAPI (blue) in NL. Merged image in **I**. White dashed lines in **H,I** indicate the borders between NL neuropil region and the adjacent glial layers. Scale bars = 200 μm in **A**; 20 μm in **B,C**; 10 μm in inset; 50 μm in **I** (applies to **D–I**).

dorsal neuropil, although the PDs calculated from individual subzones varied across cases.

In the sham-operated subjects that received midline incisions that were either caudal or rostral to the XDCT without damaging NM neurons or their axons, there was no reliable difference in the density of PMCA2 immunostaining between the dorsal and the ventral NL neuropil domains at any survival times (Fig. 7A,B). The PDs (-3.6 ± 2.1) were not significantly different from those of the unoperated control subjects, indicating that the observed decreases in PMCA2 immunoreactivity in the ventral NL neuropil following transection of XDCT were not caused by lesion-related cytotoxic events.

PMCA2 immunoreactivity in NL following unilateral cochlea removal

The eighth nerve is the only excitatory input to NM neurons. Unilateral cochlea removal eliminates excitatory action poten-

tials in both the eighth nerve and the ipsilateral NM and thus eliminates spike generation in the excitatory axons to the dorsal dendrites of the ipsilateral NL and the ventral dendrites of the contralateral NL (Fig. 5B; Born et al., 1991). Cochlear ganglion cells and NM neurons begin to die about 12–24 hours after cochlea removal, and by 48 hours about 30% NM neurons have degenerated (Rubel et al., 1990).

Immediately after the unilateral cochlea removal (0 hours), the density of PMCA2 staining showed no reliable qualitative or quantitative differences between the dorsal and the ventral neuropil domains on either side of the brain (Fig. 7A). The PD values were not significantly different from those of the unoperated control group on the ipsilateral side (-2.1 ± 9.7) or on the contralateral side (-6.1 ± 9.7). On the other hand, from 30 minutes to 14 hours following cochlea removal, the ventral neuropil contralateral to the cochlea removal exhibited a readily apparent and statistically significant decrease in

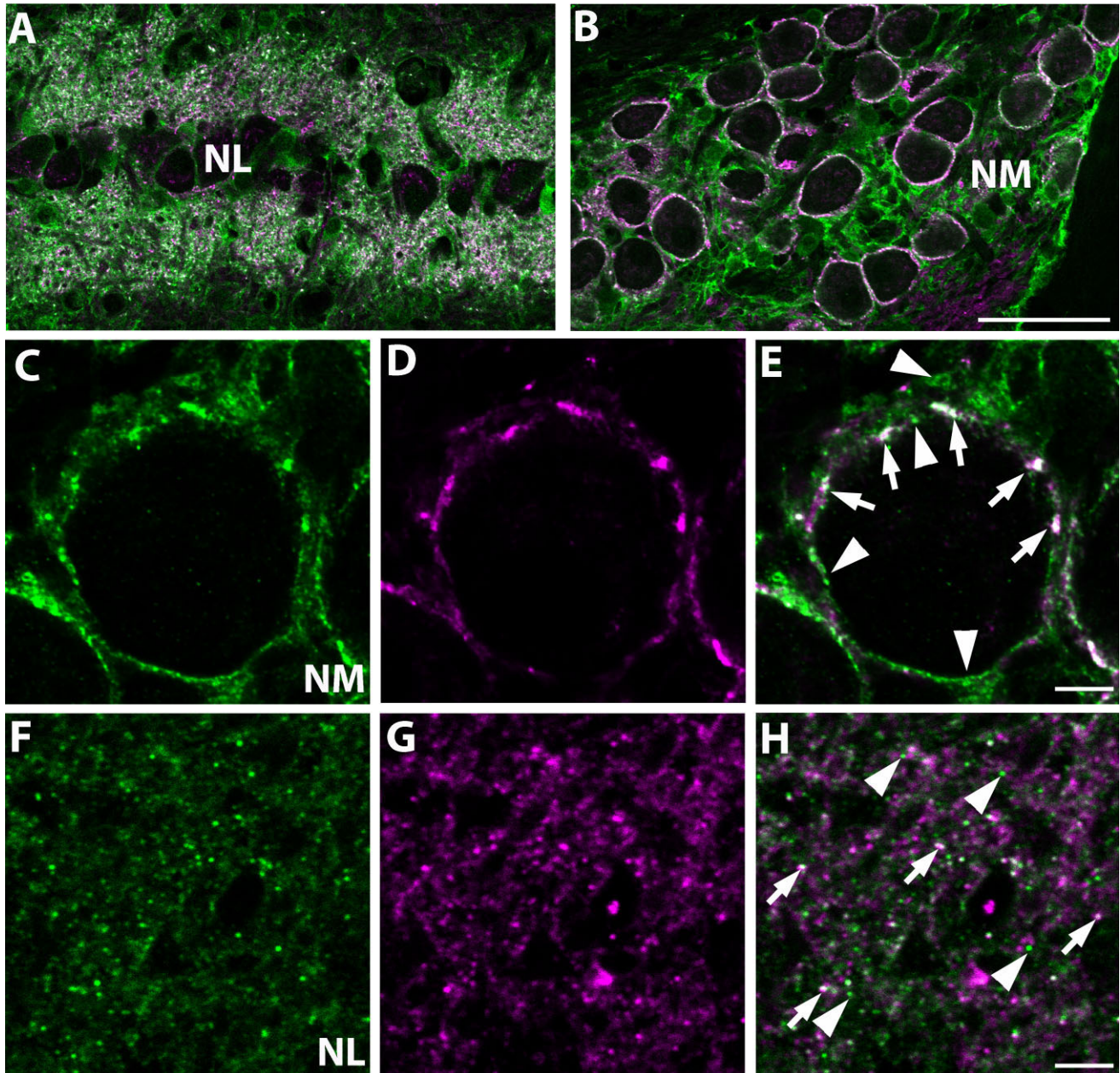


Figure 3.

Low-magnification (A,B) and high-magnification (C–H) photomicrographs of sections doubly labeled with PMCA2 (green) and the presynaptic marker SNAP-25 (magenta) in NL (A,F–H) and NM (B–E). E and H are merged images of NM neuron soma and NL neuropil region, respectively. Arrows and arrowheads indicate the subcellular components with double labeling or with single labeling for PMCA2, respectively. Scale bars = 50 μm in B (applies to A,B); 5 μm in E (applies to C–E); 7.5 μm in H (applies to F–H).

PMCA2 immunoreactivity compared with the adjacent dorsal neuropil of the same neurons (Figs. 7A, 9A,C,E), with a time course comparable to that following XDCT transection. The relative PD in the staining density was -17.6 ± 15.7 at 30 minutes, -31.1 ± 10.2 at 3 hours, -19.7 ± 5.8 at 6 hours, and -26.0 ± 9.1 at 14 hours. These PD values were all significantly less than those of the unoperated control group (P s < 0.001).

Unexpectedly, changes in PMCA2 immunoreactivity in the dorsal neuropil of the ipsilateral NL appeared smaller and less

reliable than in the ventral neuropil of the contralateral NL (Figs. 7A, 9B,D,F). Qualitative examination of the tissue did not reveal a reliable difference in the staining density between the two neuropil domains of the ipsilateral NL until 3 hours after the manipulation. Quantification and statistical analysis across all cases within individual survival groups revealed a significantly smaller PD value at 3 hours (-12.6 ± 8.2 ; $P < 0.01$) and 6 hours (-15.3 ± 10.8 ; $P < 0.01$), but not at 0.5 hours (-3.1 ± 12.9) or 14 hours (-4.5 ± 3.8), compared with the

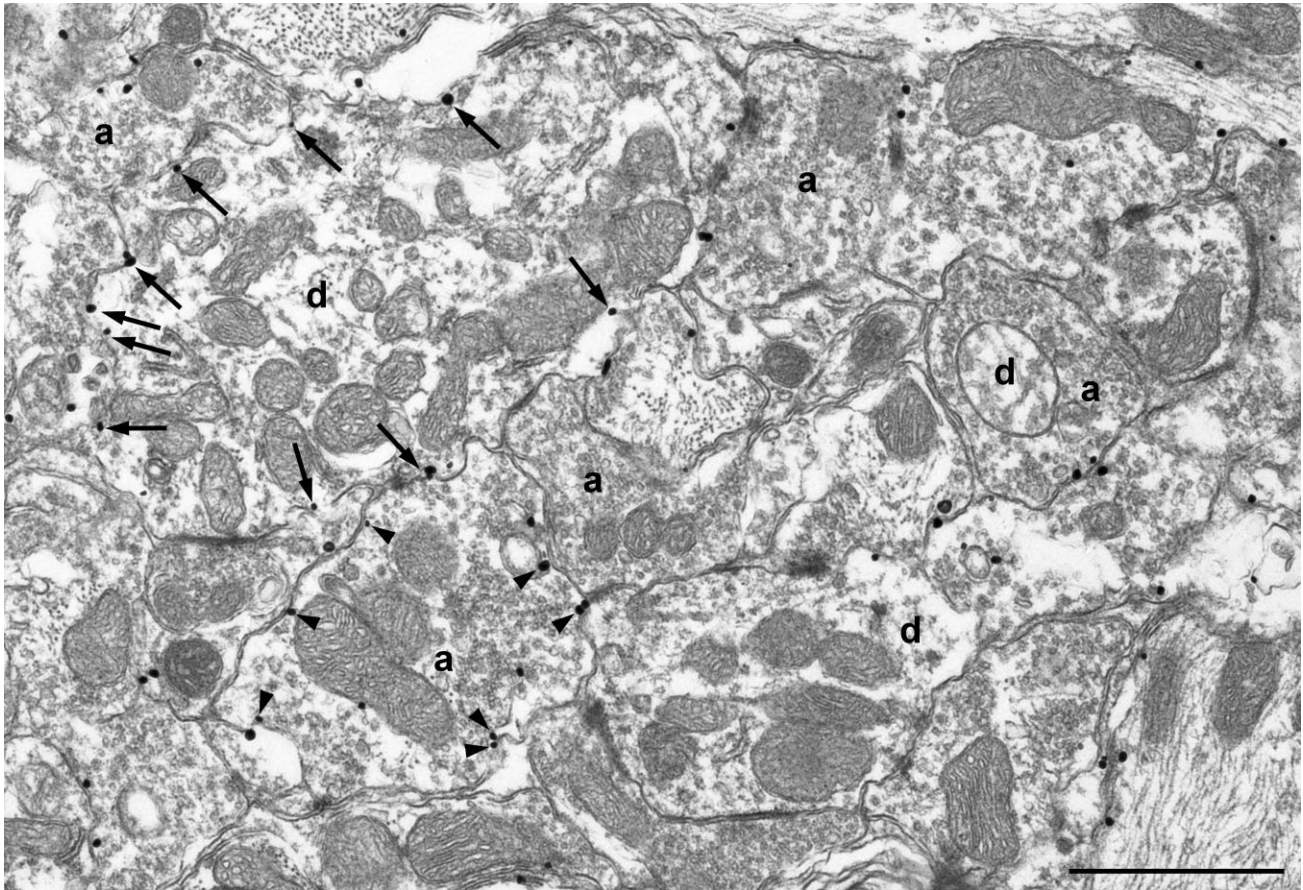


Figure 4. Transmission electron micrograph of PMCA2 immunoreactivity in NL neuropil region. Gold particles are distributed in a membrane-associated manner in both dendritic (d) and axonal (a) structures. Arrows and arrowheads point to the gold particles in a dendritic and an axonal structure, respectively. Scale bar = 1 μ m.

unoperated control group (-2.1 ± 9.7). The results of two-way ANOVA for the survival time following unilateral cochlea removal and the domain of the deprived neuropil (dorsal vs. ventral) indicated that the effect of cochlea removal on PMCA2 immunoreactivity depended on the domain of the deprived neuropil ($P < 0.0001$; Fig. 7A). A significantly greater change occurred in the deprived ventral neuropil than in the deprived dorsal neuropil within the first 14 hours following unilateral cochlea removal.

PMCA2 immunoreactivity in NL following bilateral cochlea removal

The asymmetry of the effect of unilateral cochlea removal on the deprived dorsal and ventral neuropil of NL provides a means to examine whether the elimination of activity in one neuropil domain or the loss of the balance of the activity between the two neuropil domains is responsible for the observed changes in PMCA2 immunoreactivity. If the balance of the activity is sufficient to maintain the PMCA2 immunoreactivity in NL neuropil, bilateral cochlea removal should produce no change in staining density in either domain and thus no difference between two domains. Otherwise, because of the differential effects of unilateral cochlea removal on the de-

prived dorsal and ventral neuropil, we should detect a difference of staining density between two neuropil domains following bilateral cochlea removal.

Five animals received bilateral cochlea removal and survived for 3 hours, the time point at which the most dramatic changes were found following a single operation of either XDCT transection or unilateral cochlea removal. For all five cases, the density of PMCA2 immunoreactivity in the ventral neuropil was significantly smaller than the dorsal neuropil ($P < 0.001$; Fig. 10). The PD of staining density between the ventral and the dorsal neuropil domains (-24.4 ± 3.4) was significantly smaller than that of the unoperated control group ($P < 0.001$). This difference may result, at least partially, from different levels of response of each neuropil domain to the deprivation of presynaptic activity. However, whether the breakdown of the balance of activity between two neuropil domains also contributed to the changes in PMCA2 immunoreactivity could not be determined by this comparison.

Correlation of changes in PMCA2 immunoreactivity with MAP2 immunoreactivity

To explore whether the changes in PMCA2 immunoreactivity are associated with structural changes of NL dendrites,

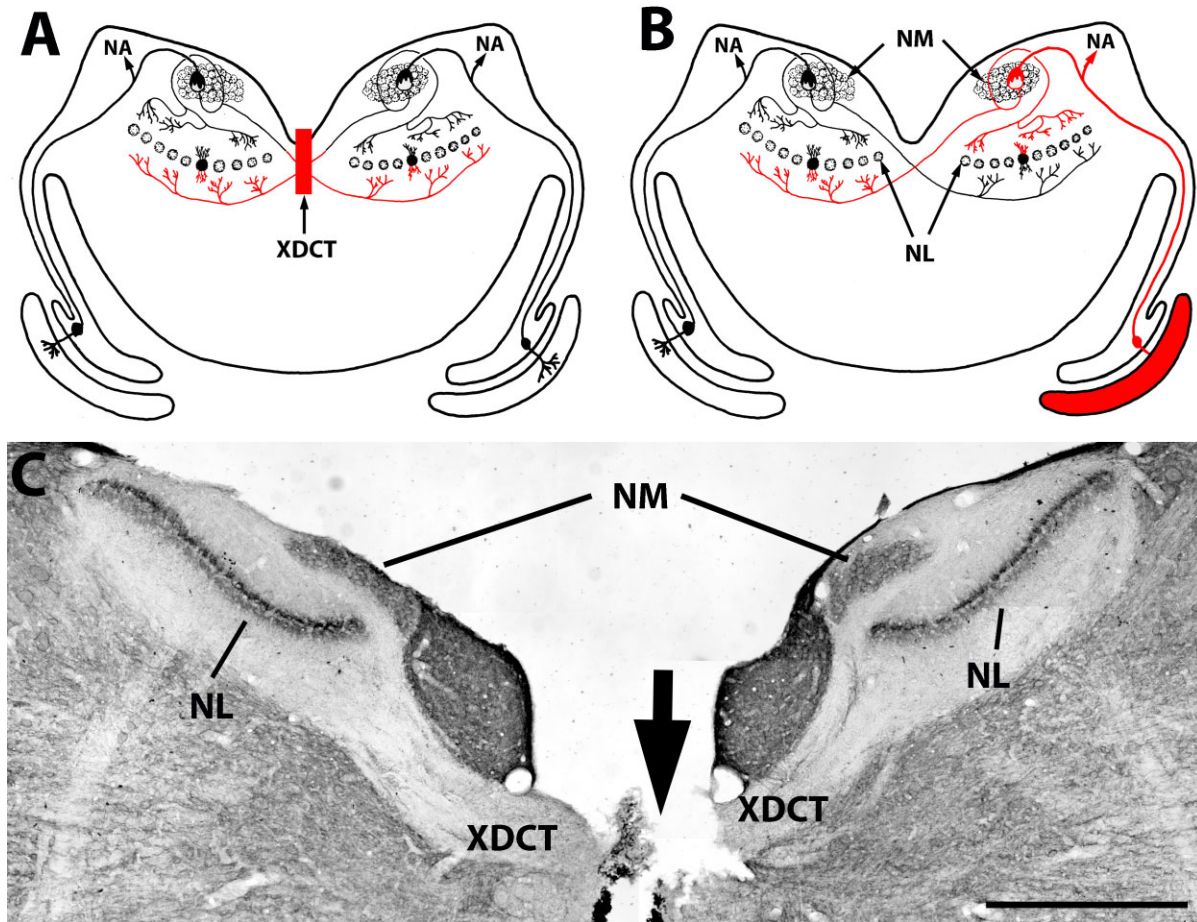


Figure 5.

Differential innervation of NL dendrites and the consequences of the surgeries. **A,B:** Schematic drawings of the chick brainstem in the coronal plane illustrate the affected dendritic fields following XDCT transection (**A**) and unilateral cochlea removal (**B**). Red indicates the surgical site for each manipulation and deafferented axons and dendrites influenced by each manipulation. **C:** Low-magnification photomicrograph illustrating a complete XDCT transection (black arrow). Note the significant difference in PMCA2 staining intensity between the dorsal and ventral neuropil regions of NL, bilaterally, 3 hours after the transection. Photomontages were constructed in **C** using Adobe Photoshop (Adobe Systems Inc., Mountain View, CA). NA, nucleus angularis. Scale bar = 500 μm .

changes in PMCA2 immunoreactivity were plotted as a function of changes in MAP2 immunoreactivity following unilateral cochlea removal (Fig. 11). The average PD of PMCA2 immunoreactivity in the contralateral NL (-16.9 ± 7.7) was significantly greater than that in the ipsilateral NL (-4.2 ± 6.1), consistent with the quantification analyses described above, although the absolute values of the PDs measured from sections with fluorescent immunocytochemical staining (Fig. 11) are smaller than those measured from sections with peroxidase staining (Fig. 7). On the other hand, the average PD of MAP2 immunoreactivity was not significantly different between the contralateral (-30.3 ± 9.9) and the ipsilateral (-35.2 ± 12.8) sides, consistent with our previous report (Wang and Rubel, 2008). Although the PDs in immunoreactivity varied among cases, those with a larger change in PMCA2 immunoreactivity tended to have a larger change in MAP2 immunoreactivity. This correlation was evident on both contralateral (Fig. 11A) and ipsilateral (Fig. 11B) sides. Post hoc linear trend analysis reveals a highly significant trend toward

increasing changes in MAP2 as a function of changes in PMCA2 ($P < 0.001$).

PMCA2 immunoreactivity in NM following unilateral cochlea removal

PMCA2 immunoreactivity in the deprived ipsilateral NM was examined following unilateral cochlea removal and compared with that in the intact contralateral NM. During the entire 14-hour observation period following the manipulation, no distinct difference between the ipsilateral and the contralateral NM was detected in either the staining pattern or the average density of the immunoreactivity (Fig. 12). Almost every neuron in NM displayed a perisomatic staining of PMCA2 before and after the manipulation. One-way ANOVA followed by post hoc comparisons revealed no significant difference in the average density of staining between the two sides measured from the middle portion of the nucleus at all survival times.

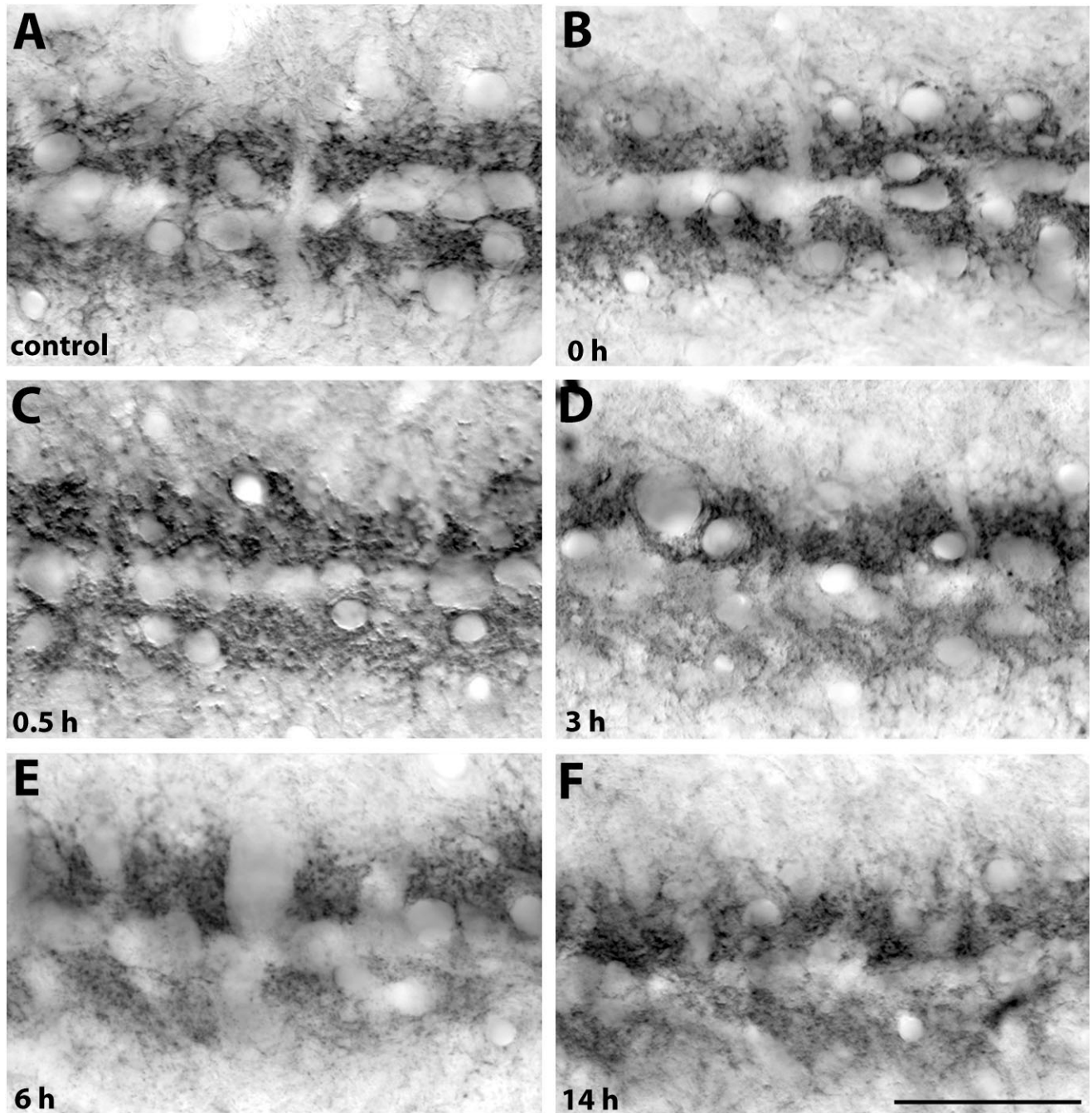


Figure 6. PMCA2 immunoreactivity in NL following XDCT transection. A was taken from an unoperated case and B–F from the animals that survived 0, 0.5, 3, 6, and 14 hours following the surgery, respectively. Note that staining intensities between the dorsal and the ventral neuropil domains appear similar in A and B and different in C–F. The ventral neuropil exhibited a lower density of staining compared with the dorsal neuropil 0.5–14 hours following the surgery. Scale bar = 50 μ m.

DISCUSSION

In this study, we demonstrate that the calcium efflux protein PMCA2 is regulated independently and/or differentially in sub-cellular compartments of individual neurons in a way that is correlated with presynaptic activity. In the chick auditory brainstem, PMCA2 immunoreactivity is rapidly and differen-

tially down-regulated in NL dendrites and/or presynaptic terminals from NM where presynaptic action potentials have been eliminated, but not in corresponding elements on the other side of the same neurons that are receiving inputs showing normal action potential rates. In addition, PMCA2 immunoreactivity in the somata of NM neurons does not appear to

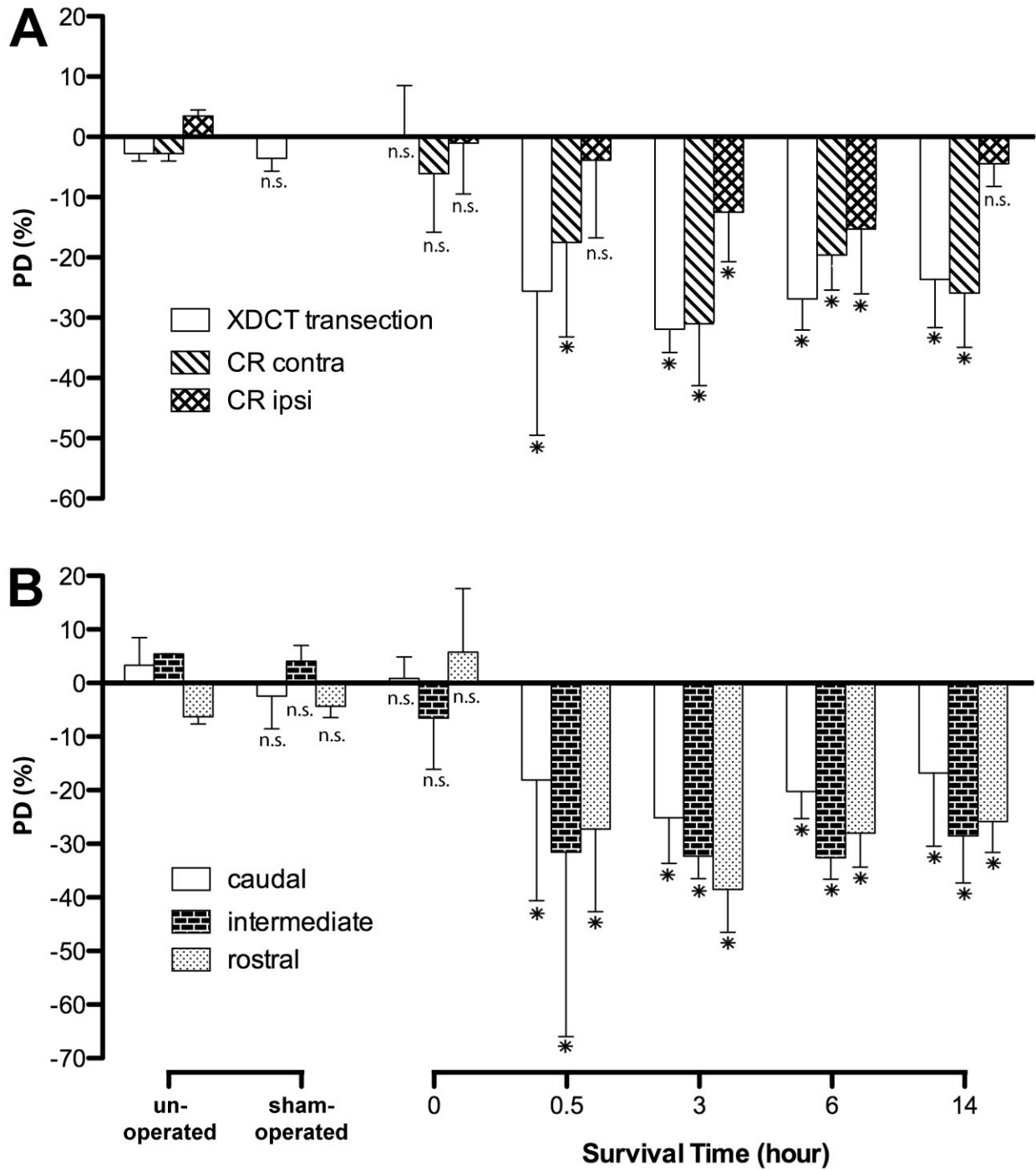


Figure 7. Time course of the average density of PMCA2 immunoreactivity in the deprived NL neuropil following manipulations. **A:** The average percentage difference (PD) across the whole NL following XDCT transection or unilateral cochlea removal. PDs were averaged from two sides of the brain following XDCT transection. **B:** PDs were measured from the caudal, intermediate, and rostral portions of the nucleus following XDCT transection. All error bars indicate SD. The asterisk and n.s. below individual bars indicate that the PD of a specific survival group or position is significantly smaller ($P < 0.05$) than or nonsignificant ($P > 0.05$) compared with the corresponding unoperated control, respectively.

be sensitive to changes in presynaptic activity induced by our manipulations. The significance of the compartmental specificity of PMCA2 regulation is discussed below in terms of its potential involvement in rapid structural changes in neuronal dendrites.

One important caveat of this study is that we cannot determine with the present analyses whether the deprivation-induced changes in PMCA2 immunoreactivity are presynaptic or postsynaptic or both. Our results and other TEM localiza-

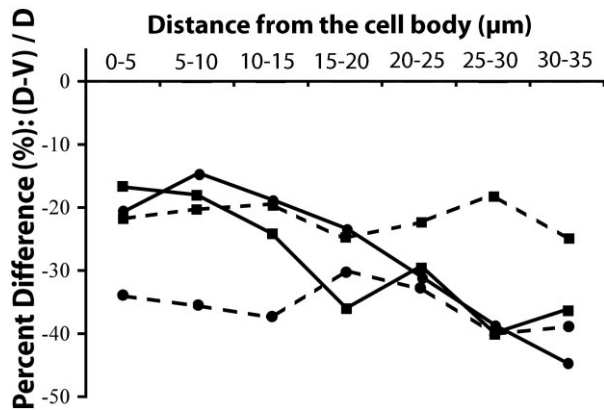


Figure 8. Four individual examples demonstrating changes in PMCA2 immunoreactivity as a function of the distance from the NL cell bodies. Animals survived for 6 hours following XDCT transection. PD values were calculated from a single section selected from the intermediate portion of NL where the dendrites extend about 35 μm dorsally and ventrally to the neuronal cell bodies. Decreases in PMCA2 immunoreactivity were detected in both the proximal and the distal portions of NL neuropil.

tion studies (Stauffer et al., 1997; Burette and Weinberg, 2007; Burette et al., 2009) clearly indicate that PMCA2 is expressed in both presynaptic and postsynaptic structures in the brain and peripheral sensory systems. However, three lines of evidence suggest that changes in PMCA2 immunoreactivity occurred at least partially in NL dendrites. First, following cochlea removal, PMCA2 immunoreactivity in NM did not show a hint of change up to 14 hours (the present study) even though the axons of the eighth nerve are beginning to degenerate by about 14 hours (Rubel et al., 1990). Second, after XDCT transection, a significant reduction of neurofilaments and microtubules was seen in the ventral NL dendrites by 4 hours, but, at that time and for several hours thereafter, no changes were noted in the ultrastructure of the NM synapses on these dendrites (Deitch and Rubel, 1989). Third, PMCA2 immunoreactivity in the dorsal and ventral NL neuropil domains showed different sensitivities to the manipulations of presynaptic activity (the present study). These observations do not prove that the observed changes in PMCA2 immunoreactivity do not take place in presynaptic structures in NL neuropil. However, they certainly suggest that the most significant changes following our manipulations, particularly at the short intervals, are taking place in the dendrites.

Time course of PMCA2 changes in NL

Loss of PMCA2 immunoreactivity does not appear to be a direct consequence of accompanying reductions in the membrane surface of NL dendrites. A significant decrease of PMCA2 immunoreactivity by 18–26% at 0.5 hours indicates a decrease in the *density* of the immunoreactivity on the dendritic surface. At this early time point, changes in the total dendritic branch length and area of NL neurons are not detectable (Deitch and Rubel, 1984; Sorensen and Rubel, 2006). At later time periods (3–14 hours), reduction in the membrane surface of NL dendrites, and presumably of NM terminals, increases over the survival time following the manipulations

(Deitch and Rubel, 1984), although little further loss of PMCA2 immunoreactivity was detected during this time period, indicating that the density of PMCA2 immunoreactivity reaches the greatest loss between 0.5 hours and 3 hours and then slowly recovers or increases by 14 hours. The initial decrease could result from degradation of PMCA2 protein, alternation of its structure and/or binding properties, or decreases in availability of the protein coupled with rapid normal turnover (Grati et al., 2006). This rapid and transient loss of a fraction of PMCA2 immunoreactivity suggests multiple pools of PMCA2 with distinct mobilities in NL or NM neurons, a pattern that has been observed in the stereocilia of hair cells (Grati et al., 2006). The later recovery of PMCA2 may be a result of up-regulation of PMCA2 by increased $[\text{Ca}^{2+}]_i$ (Guerini et al., 1999, 2005). An additional line of evidence that PMCA2 changes are not a result of structural changes comes from the occurrence of PMCA2 changes throughout the proximal-distal neuropil domain. On the other hand, dendritic branches in NL shrink preferentially in the distal portion and slightly gain length proximally (Sorensen and Rubel, 2006).

Synaptic regulation of PMCA2

The immediate loss of PMCA2 immunoreactivity is one of the earliest cellular processes in NL neuropil following deprivation of excitatory inputs, along with changes in 2-deoxyglucose uptake (Lippe et al., 1980), and occurs well before detectable structural changes (Deitch and Rubel, 1984, 1989; Wang and Rubel, 2008) and metabolism alterations (Durham and Rubel, 1985). The rapidity of changes in PMCA2 immunoreactivity, consistent with its occurrence throughout the neuropil domain, places major constraints on the cellular processes that might mediate these changes. Sham operations showed that these PMCA2 changes were not caused by lesion-related cytotoxic events to the surrounding tissue. Instead, decreases in PMCA2 immunoreactivity are likely to be activity dependent, insofar as both XDCT transection and cochlea removal cause an immediate cessation of action potentials of excitatory NM afferents to affected NL dendrites (Bom et al., 1991). Possible changes in presynaptically localized PMCA2 could be a direct consequence of changes in calcium influx through voltage-gated calcium channels. Dendritic PMCA2, on the other hand, may respond to the interruption of neurotransmission and concomitant cessation of glutamate release. Glutamate receptors that may regulate PMCA2 through a calcium-dependent mechanism include calcium-permeable AMPA and NMDA receptors and metabotropic glutamate receptors that mediate $[\text{Ca}^{2+}]_i$ through their inhibition on voltage-gated calcium channels and release from intracellular calcium stores (Zirpel and Rubel, 1996; Lu and Rubel, 2005).

In addition to glutamate receptors, activation of neurotrophin receptors may also regulate PMCA2 in NL dendrites. One unexpected observation in the current study is that changes in the density of PMCA2 immunoreactivity in deprived dorsal neuropil were significantly smaller than those in deprived ventral neuropil, indicating that PMCA2 immunoreactivity is regulated somewhat differentially in the two NL neuropil domains. These differential responses imply that other cellular pathways with varied expression and/or function between two domains may modulate the activity-dependent PMCA2 expression. Of most interest is the restricted distribution of the TrkB receptor in the ventral, but not the dorsal, NL dendrites

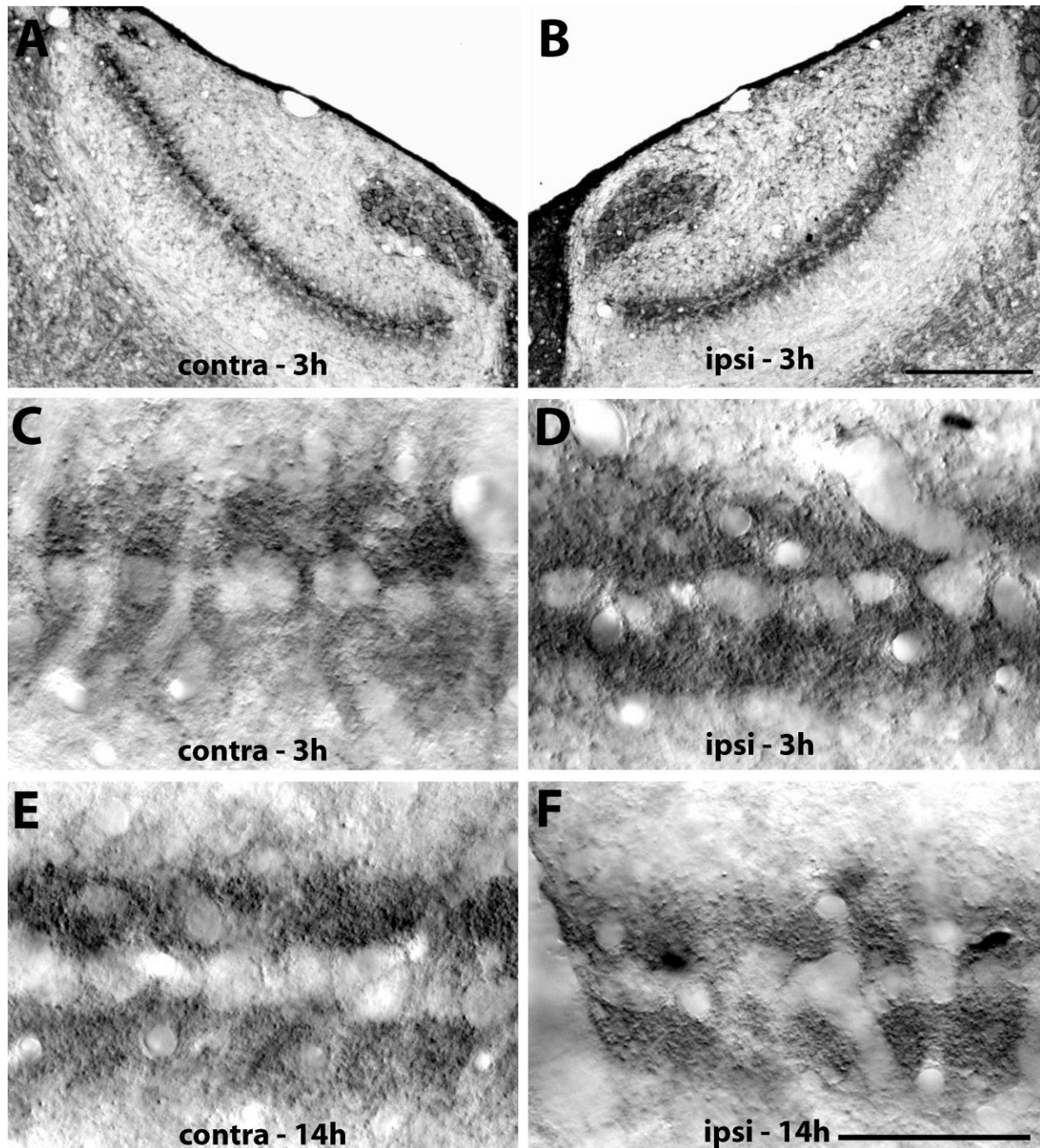


Figure 9. PMCA2 immunoreactivity in NL at 3 hours (A–D) and 14 hours (E,F) following unilateral cochlea removal. A, C, and E were taken from the side contralateral to the operated ear and B, D, and F from the side ipsilateral to the operated ear. Staining intensities between the dorsal and the ventral neuropil domains are clearly different on the contralateral side and appear comparable on the ipsilateral side. Scale bars = 200 μm in A (applies to A,B); 50 μm in F (applies to C–F).

(Cochran et al., 1999). TrkB is activated by brain-derived neurotrophic factor (BDNF) and neurotrophin-4/5 (NT-4/5) as well as by zinc, which is coreleased with glutamate (Huang et al., 2008). BDNF/TrkB signaling and other neurotrophin pathways can react rapidly to synaptic transmission and calcium signaling of postsynaptic targets and regulate postsynaptic

dendritic structure with compartmental specificity (Jiang and Guroff, 1997; Tao et al., 1998; Meyer-Franke et al., 1998; Kafitz et al., 1999; Finkbeiner, 2000; Xu et al., 2000; McAllister, 2000, 2001). It will be important to investigate whether the differential response of PMCA2 in NL is associated with activation of TrkB pathway in the ventral, but not the dorsal, dendrites.

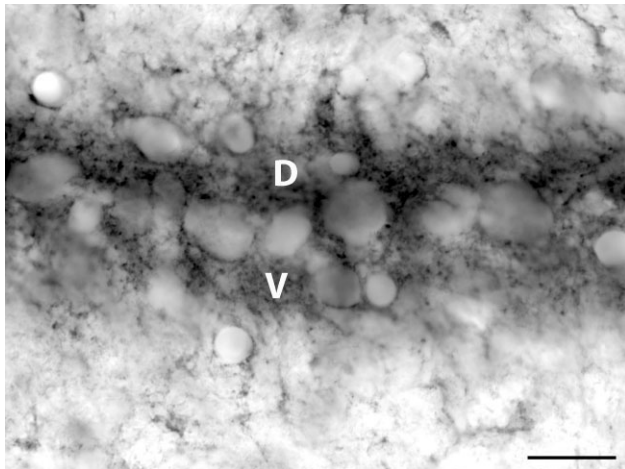


Figure 10. PMCA2 immunoreactivity in NL at 3 hours following bilateral cochlea removal. Staining intensity in the ventral neuropil (V) is notably lower than in the dorsal neuropil (D). Scale bar = 20 μ m.

PMCA2 in dendritic regulation

The temporal properties of PMCA2 changes in NL neuropil following deprivation suggest a basis for the participation of PMCA2 in subsequent subcellular and structural changes in NL dendrites. The hypothesis of structural regulation by dendritic PMCA2 is particularly attractive because of the pivotal role of intradendritic calcium signals in activity-dependent dendritic regulation, which has been proposed in a variety of neuronal systems (Lohmann et al., 2002; Wong and Ghosh, 2002; Chen and Ghosh, 2005; Lohmann and Wong, 2005; Redmond and Ghosh, 2005). For NL neurons, rapid atrophy and retraction of activity-deprived dendritic branches but not matching dendrites of the same neurons with normal inputs are likely to be a result of dynamics of local calcium signals, but not global calcium signaling that produces a delayed effect on dendritic development through gene transcription and presumably affects all dendritic branches of individual neurons (Wong and Ghosh, 2002; Redmond and Ghosh, 2005). In chick retina, blockage of calcium-induced calcium release from the endoplasmic reticulum appears to inhibit local calcium signaling, which results in dendritic retraction of ganglion neurons (Lohmann et al., 2002). NL dendrites are rich in endoplasmic reticulum (Deitch and Rubel, 1989). Insofar as local calcium signaling depends on calcium influx primarily through transmitter-mediated receptors and voltage-gated calcium channels (Redmond and Ghosh, 2005), deprivation of presynaptic activity to NL neurons may regulate local dendritic structure by calcium signaling through GluR3 flop and GluR4 flop channels, known to be the predominant AMPA receptors on NL neurons (Raman et al., 1994; Ravindranathan et al., 2000).

In cultured sympathetic neurons of the rat superior cervical ganglion, calcium signaling mediates dendritic growth in response to activity via phosphorylation of MAP2 (Vaillant et al., 2002). Decreased MAP2 immunoreactivity and microtubule loss concomitant with dendritic retraction lend some credence to the idea that calcium signaling regulates NL dendrites by a similar mechanism (Deitch and Rubel, 1989; Wang

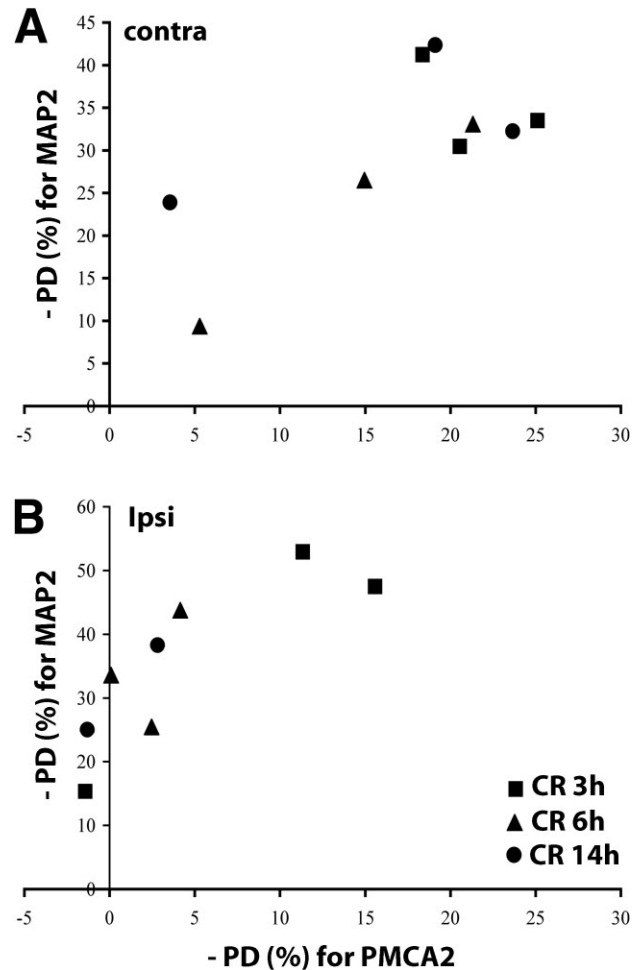


Figure 11. Correlation of changes in PMCA2 and MAP2 following unilateral cochlea removal. The average percentage difference (PD) was calculated as the change in the density of the immunoreactivity in deprived neuropil domain relative to the intact domain. CR 3h, CR 6h, and CR 14h represent 3, 6, or 14 hours following unilateral cochlea removal. Note that the changes in PMCA2 immunoreactivity in deprived ventral domain (A) are larger than those in deprived dorsal domain (B). Each data point represents an individual case. The animal with a larger change in PMCA2 immunoreactivity tended to have a larger change in MAP2 immunoreactivity.

and Rubel, 2008). The correlation of MAP2 changes with PMCA2 immunoreactivity loss in response to cochlea removal might also suggest that they are regulated by the same upstream events, and the fact that the changes in PMCA2 precede detectable changes in MAP2 and dendritic structural changes suggests an involvement of PMCA2 in regulating dendritic cytoskeleton. Alternatively, the high level of $[Ca^{2+}]_i$ that can result from PMCA2 down-regulation may regulate dendritic morphology by calcium-induced actin depolymerization, a mechanism that has been found repeatedly in hippocampal and retinal neurons (Bennett and Weeds, 1986; Rosenmund and Westbrook, 1993; Halpain et al., 1998; Job and Lagnado, 1998; Brünig et al., 2004; Cristofanilli and Akopian, 2006).

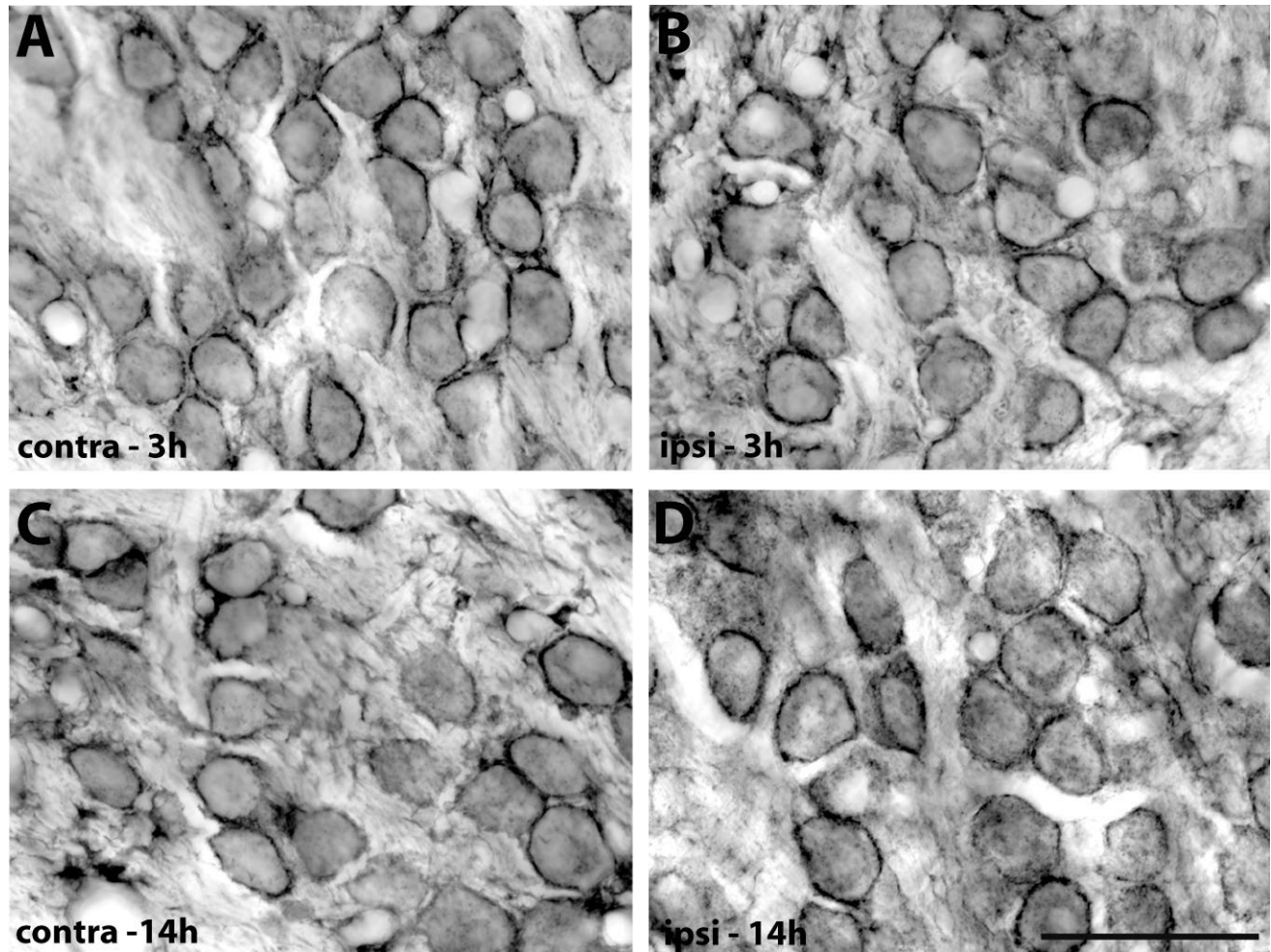


Figure 12. PMCA2 immunoreactivity in NM at 3 hours (A,B) and 14 hours (C,D) following unilateral cochlea removal. A and C were taken from the side contralateral to the operated ear and B and D from the side ipsilateral to the operated ear. Pattern and intensity of the staining in NM are similar between two sides at both survival times. Scale bar = 50 μm .

PMCA2 in presynaptic structures

As noted above, changes in PMCA2 immunoreactivity following our manipulation could occur presynaptically in NM terminals as well as in NL dendrites. Several studies have demonstrated the contribution of PMCA2 in regulating presynaptic $[\text{Ca}^{2+}]_i$ (Morgans et al., 1998; Zenisek and Matthews, 2000; Kim et al., 2005; Lnenicka et al., 2006; Johnson et al., 2007), and it is well documented that presynaptic $[\text{Ca}^{2+}]_i$ flux is critical for neurotransmitter release (Catterall and Few, 2008; Neher and Sakaba, 2008). Jensen et al. (2007) further reported that PMCA regulates excitatory synaptic transmission by showing that PMCA inhibition enhanced the frequency of the miniature excitatory postsynaptic currents in the rat hippocampal neurons and argued that this regulation is largely through PMCA2a, a fast splice variant of PMCA2. In rat hippocampal neurons, PMCA2a is located presynaptically (Jensen et al., 2007), whereas PMCA2b is postsynaptic and colocalizes with postsynaptic proteins within dendritic spines (DeMarco and Strehler, 2001). This could be the same case in the chick NM-NL synapses, as NM and NL neurons exhibit

high spontaneous and acoustic-driven discharge rates (Born et al., 1991) and presumably handle large calcium transients at least partially through a fast calcium clearance system (von Gersdorff and Borst, 2002). On the other hand, a recent immunocytochemical study in the rat brain concluded that PMCA2a concentrates in inhibitory presynaptic terminals (Burette et al., 2009). Further TEM localization studies in the chick auditory brainstem with antibodies specifically against PMCA2a or PMCA2b will be required to clarify this issue.

PMCA2 regulation: cell-type specific

It is perhaps surprising that NM did not show a discernible change in PMCA2 immunoreactivity following cochlea removal, given the fact that cochlea removal deprives both NM and NL of excitatory afferent input (Born et al., 1991). In addition, cochlea removal results in a rapid increase of $[\text{Ca}^{2+}]_i$ in all deprived NM neurons that results in the death of approximately 30% of these neurons within 2 days (Born and Rubel, 1985; Zirpel et al., 1995; Zirpel and Rubel, 1996). For a number of cell systems, PMCA has been suggested to be an important

player in calcium-mediated cell death (Garcia and Strehler, 1999; Garcia et al., 2001; Kurnellas et al., 2005). In addition, rapid decreases of PMCA message and/or protein within hours after the onset of pathological conditions have been reported from a variety of systems (Garcia et al., 1997; Ximenes et al., 2003; Nicot et al., 2003, 2005; Kip and Strehler, 2007; Herchuelz et al., 2007). We have no explanation for the failure to detect changes in PMCA2 immunoreactivity in deprived NM neurons except to suggest that presynaptic activity regulates PMCA2 in a cell-type-specific manner.

ACKNOWLEDGMENTS

We thank MacKenzie A. Howard, Armin H. Seidl, Kathryn M. Tabor, and Jason T. Sanchez for criticisms of the manuscript and Jennifer S. McCullar and Claire J. Walker for help with the Western blotting. We also thank Claire J. Walker for providing the mouse tissue.

LITERATURE CITED

- Benes FM, Parks TN, Rubel EW. 1977. Rapid dendritic atrophy following deafferentation: an EM morphometric analysis. *Brain Res* 122:1–13.
- Bennett J, Weeds A. 1986. Calcium and the cytoskeleton. *Br Med Bull* 42:385–390.
- Berod A, Hartman BK, Pujol JF. 1981. Importance of fixation in immunohistochemistry: use of formaldehyde solutions at variable pH for the localization of tyrosine hydroxylase. *J Histochem Cytochem* 29:844–850.
- Blaustein MP, Juhaszova M, Golovina VA, Church PJ, Stanley EF. 2002. Na/Ca exchanger and PMCA localization in neurons and astrocytes: functional implications. *Ann N Y Acad Sci* 976:356–366.
- Bodor AL, Katona I, Nyíri G, Mackie K, Ledent C, Hájos N, Freund TF. 2005. Endocannabinoid signaling in rat somatosensory cortex: laminar differences and involvement of specific interneuron types. *J Neurosci* 25:6845–6856.
- Born DE, Rubel EW. 1985. Afferent influences on brain stem auditory nuclei of the chicken: neuron number and size following cochlea removal. *J Comp Neurol* 231:435–445.
- Born DE, Durham D, Rubel EW. 1991. Afferent influences on brainstem auditory nuclei of the chick: nucleus magnocellularis neuronal activity following cochlea removal. *Brain Res* 557:37–47.
- Brini M, Coletto L, Pierobon N, Kraev N, Guerini D, Carafoli E. 2003. A comparative functional analysis of plasma membrane Ca^{2+} pump isoforms in intact cells. *J Biol Chem* 278:24500–24508.
- Brüning I, Kaech S, Brinkhaus H, Oertner TG, Matus A. 2004. Influx of extracellular calcium regulates actin-dependent morphological plasticity in dendritic spines. *Neuropharmacology* 47:669–676.
- Burette A, Weinberg RJ. 2007. Perisynaptic organization of plasma membrane calcium pumps in cerebellar cortex. *J Comp Neurol* 500:1127–1135.
- Burette AC, Strehler EE, Weinberg RJ. 2009. “Fast” plasma membrane calcium pump PMCA2a concentrates in GABAergic terminals in the adult rat brain. *J Comp Neurol* 512:500–513.
- Burger RM, Rubel EW. 2008. Encoding of interaural timing for binaural hearing. In: Dallos P, Oertel D, editors. *The senses: a comprehensive reference*. San Diego: Academic Press, p 613–630.
- Carafoli E. 1987. Intracellular calcium homeostasis. *Annu Rev Biochem* 56:395–433.
- Carr CE, Konishi M. 1988. Axonal delay lines for time measurement in the owl's brainstem. *Proc Natl Acad Sci U S A* 85:8311–8315.
- Carr CE, Konishi M. 1990. A circuit for detection of interaural time differences in the brain stem of the barn owl. *J Neurosci* 10:3227–3246.
- Catterall WA, Few AP. 2008. Calcium channel regulation and presynaptic plasticity. *Neuron* 59:882–901.
- Chen Y, Ghosh A. 2005. Regulation of dendritic development by neuronal activity. *J Neurobiol* 64:4–10.
- Chen Y, Wang PY, Ghosh A. 2005. Regulation of cortical dendrite development by Rap1 signaling. *Mol Cell Neurosci* 28:215–228.
- Cline HT. 2001. Dendritic arbor development and synaptogenesis. *Curr Opin Neurobiol* 11:118–126.
- Cochran SL, Stone JS, Birmingham-McDonogh O, Akers SR, Lefcort F, Rubel EW. 1999. Ontogenetic expression of trk neurotrophin receptors in the chick auditory system. *J Comp Neurol* 413:271–288.
- Conlee JW, Parks TN. 1983. Late appearance and deprivation-sensitive growth of permanent dendrites in the avian cochlear nucleus (nuc. magnocellularis). *J Comp Neurol* 217:216–226.
- Cristofanilli M, Akopian A. 2006. Calcium channel and glutamate receptor activities regulate actin organization in salamander retinal neurons. *J Physiol* 575:543–554.
- Deitch JS, Rubel EW. 1984. Afferent influences on brain stem auditory nuclei of the chicken: time course and specificity of dendritic atrophy following deafferentation. *J Comp Neurol* 229:66–79.
- Deitch JS, Rubel EW. 1989. Rapid changes in ultrastructure during deafferentation-induced dendritic atrophy. *J Comp Neurol* 281:234–258.
- DeMarco SJ, Strehler EE. 2001. Plasma membrane Ca^{2+} -atpase isoforms 2b and 4b interact promiscuously and selectively with members of the membrane-associated guanylate kinase family of PDZ (PSD95/Dlg/ZO-1) domain-containing proteins. *J Biol Chem* 276:21594–21600.
- Duman JG, Chen L, Hille B. 2008. Calcium transport mechanisms of PC12 cells. *J Gen Physiol* 131:307–323.
- Durham D, Rubel EW. 1985. Afferent influences on brain stem auditory nuclei of the chicken: changes in succinate dehydrogenase activity following cochlea removal. *J Comp Neurol* 231:446–456.
- Elwess NL, Filoteo AG, Enyedi A, Penniston JT. 1997. Plasma membrane Ca^{2+} pump isoforms 2a and 2b are unusually responsive to calmodulin and Ca^{2+} . *J Biol Chem* 272:17981–17986.
- Finkbeiner S. 2000. Calcium regulation of the brain-derived neurotrophic factor gene. *Cell Mol Life Sci* 57:394–401.
- Fresu L, Dehpour A, Genazzani AA, Carafoli E, Guerini D. 1999. Plasma membrane calcium ATPase isoforms in astrocytes. *Glia* 28:150–155.
- Garcia ML, Strehler EE. 1999. Plasma membrane calcium ATPases as critical regulators of calcium homeostasis during neuronal cell function. *Front Biosci* 4:D869–D882.
- Garcia ML, Murray KD, Garcia VB, Strehler EE, Isackson PJ. 1997. Seizure-induced alterations of plasma membrane calcium ATPase isoforms 1, 2 and 3 mRNA and protein in rat hippocampus. *Brain Res Mol Brain Res* 45:230–238.
- Garcia ML, Usachev YM, Thayer SA, Strehler EE, Windebank AJ. 2001. Plasma membrane calcium ATPase plays a role in reducing Ca^{2+} -mediated cytotoxicity in PC12 cells. *J Neurosci Res* 64:661–669 [erratum in *J Neurosci Res* 66:733–735].
- Grati M, Schneider ME, Lipkow K, Strehler EE, Wenthold RJ, Kachar B. 2006. Rapid turnover of stereocilia membrane proteins: evidence from the trafficking and mobility of plasma membrane Ca^{2+} -ATPase 2. *J Neurosci* 26:6386–6395.
- Guerini D, Garcia-Martin E, Gerber A, Volbracht C, Leist M, Merino CG, Carafoli E. 1999. The expression of plasma membrane Ca^{2+} pump isoforms in cerebellar granule neurons is modulated by Ca^{2+} . *J Biol Chem* 274:1667–1676.
- Guerini D, Coletto L, Carafoli E. 2005. Exporting calcium from cells. *Cell Calcium* 38:281–289.
- Halpain S, Hipolito A, Saffer L. 1998. Regulation of F-actin stability in dendritic spines by glutamate receptors and calcineurin. *J Neurosci* 18:9835–9844.
- Harris RM, Woolsey TA. 1981. Dendritic plasticity in mouse barrel cortex following postnatal vibrissa follicle damage. *J Comp Neurol* 96:357–376.
- Herchuelz A, Kamagate A, Ximenes H, Van Eylen F. 2007. Role of Na/Ca exchange and the plasma membrane Ca^{2+} -ATPase in beta cell function and death. *Ann N Y Acad Sci* 1099:456–467.
- Hille B. 1994. Modulation of ion-channel function by G-protein-coupled receptors. *Trends Neurosci* 17:531–536.
- Huang YZ, Pan E, Xiong ZQ, McNamara JO. 2008. Zinc-mediated transactivation of TrkB potentiates the hippocampal mossy fiber-CA3 pyramidal synapse. *Neuron* 57:546–558.
- Jensen TP, Filoteo AG, Knopfel T, Empson RM. 2007. Presynaptic plasma membrane Ca^{2+} ATPase isoform 2a regulates excitatory synaptic transmission in rat hippocampal CA3. *J Physiol* 579:85–99.
- Jiang H, Guroff G. 1997. Actions of the neurotrophins on calcium uptake. *J Neurosci Res* 50:355–360.
- Job C, Lagnado L. 1998. Calcium and protein kinase C regulate the actin

- cytoskeleton in the synaptic terminal of retinal bipolar cells. *J Cell Biol* 143:1661–1672.
- Johnson JE Jr, Perkins GA, Giddabasappa A, Chaney S, Xiao W, White AD, Brown JM, Waggoner J, Ellisman MH, Fox DA. 2007. Spatiotemporal regulation of ATP and Ca^{2+} dynamics in vertebrate rod and cone ribbon synapses. *Mol Vis* 13:887–919.
- Joseph AW, Hyson RL. 1993. Coincidence detection by binaural neurons in the chick brain stem. *J Neurophysiol* 69:1197–1211.
- Kafitz KW, Rose CR, Thoenen H, Konnerth A. 1999. Neurotrophin-evoked rapid excitation through TrkB receptors. *Nature* 401:918–921.
- Kim MH, Korogod N, Schneggenburger R, Ho WK, Lee SH. 2005. Interplay between Na^{+}/Ca^{2+} exchangers and mitochondria in Ca^{2+} clearance at the calyx of Held. *J Neurosci* 25:6057–6065.
- Kip SN, Strehler EE. 2007. Rapid downregulation of NCX and PMCA in hippocampal neurons following H_2O_2 oxidative stress. *Ann N Y Acad Sci* 1099:436–439.
- Kurnellas MP, Nicot A, Shull GE, Elkabes S. 2005. Plasma membrane calcium ATPase deficiency causes neuronal pathology in the spinal cord: a potential mechanism for neurodegeneration in multiple sclerosis and spinal cord injury. *FASEB J* 19:298–300.
- Lippe WR, Steward O, Rubel EW. 1980. The effect of unilateral basilar papilla removal upon nuclei laminaris and magnocellularis of the chick examined with [3H]2-deoxy-D-glucose autoradiography. *Brain Res* 196:43–58.
- Lnenicka GA, Grizzaffi J, Lee B, Rumpal N. 2006. Ca^{2+} dynamics along identified synaptic terminals in drosophila larvae. *J Neurosci* 26:12283–12293.
- Lohmann C, Wong RO. 2005. Regulation of dendritic growth and plasticity by local and global calcium dynamics. *Cell Calcium* 37:403–409.
- Lohmann C, Myhr KL, Wong RO. 2002. Transmitter-evoked local calcium release stabilizes developing dendrites. *Nature* 418:177–181.
- Lu Y, Rubel EW. 2005. Activation of metabotropic glutamate receptors inhibits high-voltage-gated calcium channel currents of chicken nucleus magnocellularis neurons. *J Neurophysiol* 93:1418–1428.
- Meyer-Franke A, Wilkinson GA, Kruttgen A, Hu M, Munro E, Hanson MG Jr, Reichardt LF, Barres BA. 1998. Depolarization and cAMP elevation rapidly recruit TrkB to the plasma membrane of CNS neurons. *Neuron* 21:681–693.
- McAllister AK. 2000. Cellular and molecular mechanisms of dendrite growth. *Cereb Cortex* 10:963–973.
- McAllister AK. 2001. Neurotrophins and neuronal differentiation in the central nervous system. *Cell Mol Life Sci* 58:1054–1060.
- McCullough BJ, Tempel BL. 2004. Haplo-insufficiency revealed in deaf-waddler mice when tested for hearing loss and ataxia. *Hear Res* 195:90–102.
- Morgans CW, El Far O, Berntson A, Wassle H, Taylor WR. 1998. Calcium extrusion from mammalian photoreceptor terminals. *J Neurosci* 18:2467–2474.
- Neher E, Sakaba T. 2008. Multiple roles of calcium ions in the regulation of neurotransmitter release. *Neuron* 59:861–872.
- Nicot A, Ratnakar PV, Ron Y, Chen CC, Elkabes S. 2003. Regulation of gene expression in experimental autoimmune encephalomyelitis indicates early neuronal dysfunction. *Brain* 126:398–412.
- Nicot A, Kurnellas M, Elkabes S. 2005. Temporal pattern of plasma membrane calcium ATPase 2 expression in the spinal cord correlates with the course of clinical symptoms in two rodent models of autoimmune encephalomyelitis. *Eur J Neurosci* 21:2660–2670.
- Nimchinsky EA, Sabatini BL, Svoboda K. 2002. Structure and function of dendritic spines. *Annu Rev Physiol* 64:313–353.
- Overholt EM, Rubel EW, Hyson RL. 1992. A circuit for coding interaural time differences in the chick brainstem. *J Neurosci* 12:1698–1708.
- Parks TN, Rubel EW. 1975. Organization and development of brain stem auditory nuclei of the chicken: organization of projections from n. magnocellularis to n. laminaris. *J Comp Neurol* 164:435–448.
- Raman IM, Zhang S, Trussell LO. 1994. Pathway-specific variants of AMPA receptors and their contribution to neuronal signaling. *J Neurosci* 14:4998–5010.
- Ravindranathan A, Donevan SD, Sugden SG, Greig A, Rao MS, Parks TN. 2000. Contrasting molecular composition and channel properties of AMPA receptors on chick auditory and brainstem motor neurons. *J Physiol* 523:667–684.
- Redmond L, Ghosh A. 2005. Regulation of dendritic development by calcium signaling. *Cell Calcium* 37:411–416.
- Rosenmund C, Westbrook GL. 1993. Calcium-induced actin depolymerization reduces NMDA channel activity. *Neuron* 10:805–814.
- Rubel EW, Hyson RL, Durham D. 1990. Afferent regulation of neurons in the brain stem auditory system. *J Neurobiol* 21:169–196.
- Sepúlveda MR, Hidalgo-Sánchez M, Marcos D, Mata AM. 2007. Developmental distribution of plasma membrane Ca^{2+} -ATPase isoforms in chick cerebellum. *Dev Dyn* 236:1227–1236.
- Smith ZD. 1981. Organization and development of brain stem auditory nuclei of the chicken: dendritic development in N. laminaris. *J Comp Neurol* 203:309–333.
- Sorensen SA, Rubel EW. 2006. The level and integrity of synaptic input regulates dendrite structure. *J Neurosci* 26:1539–1550.
- Stauffer TP, Guerini D, Celio MR, Carafoli E. 1997. Immunolocalization of the plasma membrane Ca^{2+} pump isoforms in the rat brain. *Brain Res* 748:21–29.
- Street VA, McKee-Johnson JW, Fonseca RC, Tempel BL, Noben-Trauth K. 1998. Mutations in a plasma membrane Ca^{2+} -ATPase gene cause deafness in deafwaddler mice. *Nat Genet* 19:390–394.
- Tao X, Finkbeiner S, Arnold DB, Shaywitz AJ, Greenberg ME. 1998. Ca^{2+} influx regulates BDNF transcription by a CREB family transcription factor-dependent mechanism. *Neuron* 20:709–726.
- Tempel BL, Shilling DJ. 2007. The plasma membrane calcium ATPase and disease. *Subcell Biochem* 45:365–383.
- Thayer SA, Usachev YM, Pottorf WJ. 2002. Modulating Ca^{2+} clearance from neurons. *Front Biosci* 7:d1255–1279.
- Vaillant AR, Zanassi P, Walsh GS, Aumont A, Alonso A, Miller FD. 2002. Signaling mechanisms underlying reversible, activity-dependent dendrite formation. *Neuron* 34:985–998.
- Van Aelst L, Cline HT. 2004. Rho GTPases and activity-dependent dendrite development. *Curr Opin Neurobiol* 14:297–304.
- von Gersdorff H, Borst JG. 2002. Short-term plasticity at the calyx of held. *Nat Rev Neurosci* 3:53–64.
- Wang Y, Rubel EW. 2008. Rapid regulation of microtubule-associated protein 2 in dendrites of nucleus laminaris of the chick following deprivation of afferent activity. *Neuroscience* 154:381–389.
- Wong RO, Ghosh A. 2002. Activity-dependent regulation of dendritic growth and patterning. *Nat Rev Neurosci* 3:803–812.
- Ximenes HM, Kamagate A, Van Eylen F, Carpinelli A, Herchuelz A. 2003. Opposite effects of glucose on plasma membrane Ca^{2+} -ATPase and Na/Ca exchanger transcription, expression, and activity in rat pancreatic beta-cells. *J Biol Chem* 278:22956–22963.
- Xu B, Zang K, Ruff NL, Zhang YA, McConnell SK, Stryker MP, Reichardt LF. 2000. Cortical degeneration in the absence of neurotrophin signaling: dendritic retraction and neuronal loss after removal of the receptor TrkB. *Neuron* 26:233–245.
- Young SR, Rubel EW. 1983. Frequency-specific projections of individual neurons in chick brainstem auditory nuclei. *J Neurosci* 3:1373–1378.
- Young SR, Rubel EW. 1986. Embryogenesis of arborization pattern and topography of individual axons in N. laminaris of the chicken brain stem. *J Comp Neurol* 254:425–459.
- Yuste R, Bonhoeffer T. 2001. Morphological changes in dendritic spines associated with long-term synaptic plasticity. *Annu Rev Neurosci* 24:1071–1089.
- Zenisek D, Matthews G. 2000. The role of mitochondria in presynaptic calcium handling at a ribbon synapse. *Neuron* 25:229–237.
- Zirpel L, Rubel EW. 1996. Eighth nerve activity regulates the intracellular calcium concentration of cochlear nucleus neurons in the embryonic chick via a metabotropic glutamate receptor. *J Neurophysiol* 76:4127–4139.
- Zirpel L, Lachica EA, Lippe WR. 1995. Deafferentation increases the intracellular calcium of cochlear nucleus neurons in the embryonic chick. *J Neurophysiol* 74:1355–1357.